

Ligand-to-Metal Charge-Transfer Photophysics and Photochemistry of Emissive d^0 Titanocenes: A Spectroscopic and Computational Investigation

Henry C. London, Thomas J. Whittemore, Ariel G. Gale, Colin D. McMillen, David Y. Pritchett, Alexis R. Myers, Hannah D. Thomas, George C. Shields,* and Paul S. Wagenknecht*

Cite This: *Inorg. Chem.* 2021, 60, 14399–14409

Read Online

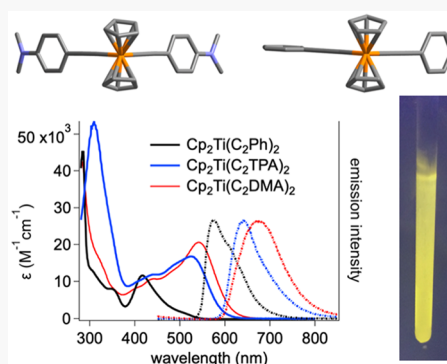
ACCESS |

Metrics & More

Article Recommendations

Supporting Information

ABSTRACT: Complexes with ligand-to-metal charge-transfer (LMCT) excited states involving d^0 metals represent a new design for photocatalysts. Herein, the photochemistry and photophysics of d^0 titanocenes of the type $\text{Cp}_2\text{Ti}(\text{C}_2\text{R})_2$, where C_2R = ethynylphenyl (C_2Ph), 4-ethynyl-dimethylaniline (C_2DMA), or 4-ethynyl-triphenylamine (C_2TPA), have been investigated. $\text{Cp}_2\text{Ti}(\text{C}_2\text{Ph})_2$ and $\text{Cp}_2\text{Ti}(\text{C}_2\text{DMA})_2$ have also been characterized by single-crystal X-ray diffraction. The two aryl rings in $\text{Cp}_2\text{Ti}(\text{C}_2\text{DMA})_2$ are nearly face-to-face in the solid state, whereas they are mutually perpendicular for $\text{Cp}_2\text{Ti}(\text{C}_2\text{Ph})_2$. All three complexes are brightly emissive at 77 K but photodecompose at room temperature when irradiated into their lowest-energy absorption band. The emission wavelengths and photodecomposition quantum yields are as follows: $\text{Cp}_2\text{Ti}(\text{C}_2\text{Ph})_2$, 575 nm and 0.65; $\text{Cp}_2\text{Ti}(\text{C}_2\text{TPA})_2$, 642 nm and 0.42; $\text{Cp}_2\text{Ti}(\text{C}_2\text{DMA})_2$, 672 nm and 0.25. Extensive benchmarking of the density functional theory (DFT) model against the structural data and of the time-dependent DFT (TDDFT) model against the absorption and emission data was performed using combinations of 13 different functionals and 4 basis sets. The model that predicted the absorption and emission data with the greatest fidelity utilized MN15/LANL2DZ for both the DFT optimization and the TDDFT. Computational analysis shows that absorption involves a transition to a $^1\text{LMCT}$ state. Whereas the spectroscopic data for $\text{Cp}_2\text{Ti}(\text{C}_2\text{TPA})_2$ and $\text{Cp}_2\text{Ti}(\text{C}_2\text{DMA})_2$ are well modeled using the optimized structure of these complexes, $\text{Cp}_2\text{Ti}(\text{C}_2\text{Ph})_2$ required averaging of the spectra from multiple rotamers involving rotation of the Ph rings. Consistent with this finding, an energy scan of all rotamers showed a very flat energetic surface, with less than 1.3 kcal/mol separating the minimum and maximum. The computational data suggest that emission occurs from a $^3\text{LMCT}$ state. Optimization of the $^3\text{LMCT}$ state demonstrates compression of the C–Ti–C bond angle, consistent with the known products of photodecomposition.



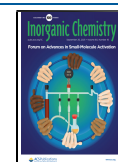
INTRODUCTION

Transition-metal complexes with metal-to-ligand charge-transfer (MLCT) excited states have been exploited for their applications in solar energy conversion^{1–3} and photoredox catalysis.^{4,5} The long excited-state lifetimes and photostability of complexes of second- and third-row transition metals (e.g., Ru^{II} ,^{1,2,4,5} Re^{I} ,^{6,7} Rh^{II} ,⁸ Ir^{III} ,⁴ and Pt^{II} ,^{4,6,7}) are particularly attractive in these applications. Complexes of first-row transition metals typically do not perform as well as their second- and third-row counterparts because of the presence of low-lying, thermally accessible metal-centered (MC) states. These thermally accessible MC states are well-known to lead to fast, radiationless mechanisms of excited-state deactivation, including decomposition.⁹ Despite the fact that some first-row transition-metal complexes have been developed with performance characteristics approaching those of parallel second- and third-row transition-metal sensitizers,^{10–17} the development of base-metal photocatalysts remains a challenge.¹⁸

Although complexes with ligand-to-metal charge-transfer (LMCT) excited states are rarely emissive in a room-temperature fluid solution and thus have found little application as photoredox catalysts, very recent reports have demonstrated that LMCT states in d^0 transition-metal complexes are excellent candidates for photoredox catalysts.^{19–22} This is due to the lack of MC excited states, which results from the absence of d electrons. For example, emission from several Zr^{IV} complexes has recently been reported, e.g., an *ansa*-zirconocene complex,^{23,24} a zirconium(IV) pyridine dipyrrolole complex (Figure 1),^{20,21} and a Zr^{IV}

Received: July 19, 2021

Published: September 8, 2021



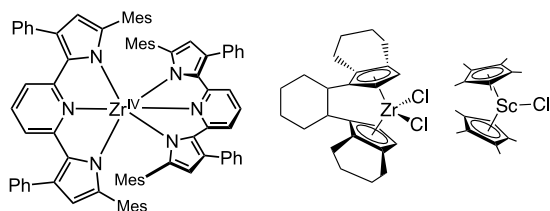


Figure 1. Complexes of d^0 metals that are emissive in a room-temperature fluid solution from their $^3\text{LMCT}$ state.

N-heterocyclic carbene complex.²² The zirconium(IV) pyridine dipyrrolide complex has also served as a photoredox catalyst. Furthermore, emission in a room-temperature fluid solution from Cp^*_2ScCl (Figure 1) has been ascribed to a Cl-to-Sc LMCT state.²⁵ These cases suggest that, with the proper design considerations, long-lived emissive excited states involving LMCT transitions in d^0 complexes of first-row transition metals (e.g., Ti and Sc) should be possible, and such complexes may serve as photoredox catalysts.

Our group recently investigated a series of titanocene complexes with absorption bands involving CT to Ti^{IV} (Figure 2).^{26–30} For example, titanocenes with ethynylferrocene

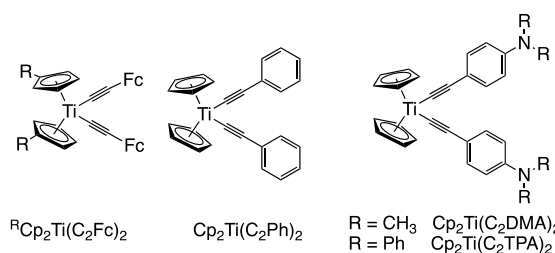


Figure 2. Titanocenes with absorption bands involving CT to Ti^{IV} , along with abbreviations used herein. DMA and TPA are used to refer to the dimethylaniline and triphenylamine substituents, respectively.

ligands, e.g., $\text{Cp}_2\text{Ti}(\text{C}_2\text{Fc})_2$, have a low-energy visible absorbance band ascribed to Fe^{II} -to- Ti^{IV} metal-to-metal charge transfer (MMCT).²⁶ Titanocenes with alkynylarylamine ligands have a low-energy absorbance ascribed to a LMCT.²⁷ In the case of MMCT from ferrocene ligands, the presence of MC states clearly impacts the excited-state lifetimes of the MMCT states, as demonstrated by time-resolved transient-absorption spectroscopy and time-dependent density functional theory (TDDFT) investigations.²⁹ Thus, we have turned our attention to the complexes with organic amine donor ligands appended to titanocenes. Our previous communication on these complexes reported on their absorption spectra and lack of photostability.²⁷ Herein, we report on their room-temperature solution-phase photochemistry, their low-temperature emission properties, and an in-depth computational investigation. Key conclusions from this investigation are that emission occurs from the $^3\text{LMCT}$ state and that this state appears to be distorted along a probable reaction coordinate for room-temperature photodecomposition. Furthermore, the rotational dynamics of the phenyl substituent in $\text{Cp}_2\text{Ti}(\text{C}_2\text{Ph})_2$ were shown to be important in modeling the absorption spectrum. To our knowledge, this is the first demonstration of summing the rotamer spectra in freely rotating systems to obtain a reasonable match for the experimental absorption spectrum. Lastly, the reaction coordinate for photodecomposition suggests strategies for photostabilization.

EXPERIMENTAL SECTION

Materials and Methods. The complexes $\text{Cp}_2\text{Ti}(\text{C}_2\text{Ph})_2$, $\text{Cp}_2\text{Ti}(\text{C}_2\text{DMA})_2$, and $\text{Cp}_2\text{Ti}(\text{C}_2\text{TPA})_2$ were prepared according to literature procedures.²⁷ UV–vis absorption spectra were recorded using a Cary-50 spectrophotometer with the cell holder thermostated to 20 °C using a Quantum Northwest TLC-50 cuvette holder. Emission spectra were recorded using a Horiba Fluorolog-3 spectrofluorimeter equipped with either a FL-1013 liquid-nitrogen dewar assembly or a J-1933 solid-sample holder.

Computational Methods. *Gaussian 16*³¹ was used for all DFT and TDDFT calculations. For each computational model, the geometry was optimized and the structure checked to be a minimum based on the frequency calculation, unless redundant coordinates were used to minimize a rotamer that was not at a minimum. *GaussView*, version 6,³² was used for all orbital imaging. Benchmarking efforts involved the functionals B3LYP,³³ B3PW91,³⁴ B97D3,³⁵ ωB97XD ,³⁶ CAM-B3LYP,³⁷ M05,³⁸ M06,³⁹ M06-L,³⁹ M11,⁴⁰ SOGGA11,⁴¹ MN12SX,⁴² N12SX,⁴³ and MN15⁴⁴ and the basis sets 6-31G(d),⁴⁵ 6-311+G(d),⁴⁶ LANL2DZ,⁴⁷ and def2-TZV.⁴⁸

X-ray Diffraction. Single crystals of $\text{Cp}_2\text{Ti}(\text{C}_2\text{Ph})_2$ and $\text{Cp}_2\text{Ti}(\text{C}_2\text{DMA})_2$ were grown by slow evaporation from a solution of the complexes in tetrahydrofuran (THF) containing 5% triethylamine. Single-crystal X-ray diffraction data were collected at 100 K using a Bruker D8 Venture diffractometer with Mo $K\alpha$ radiation ($\lambda = 0.71073$ Å) and a Photon 2 detector. Instrument control, data processing (SAINT), scaling, and absorption correction (SADABS, multiscan) were performed using the *Apex 3* software suite.⁴⁹ Space group determination (XPREP), structure solution by intrinsic phasing (SHELXT), and structure refinement by full-matrix least-squares techniques on F^2 (SHELXL) were performed using the *SHELXTL* software package.⁵⁰ All non-H atoms were refined anisotropically. H atoms attached to C atoms were placed in geometrically optimized positions using the appropriate riding models. Further details of the refinement and crystallographic data are given in the Supporting Information and are available through the Cambridge Crystallographic Data Centre as CCDC 2095566 and 2095567.

Quantum Yields. Complexes were irradiated at the selected wavelengths using a Xe short-arc lamp (Ushio UXL-450S-O) and a monochromator (SPEX 1681B; 0.22 m; 4 and 1 mm entrance and exit slits, respectively). The beam was focused to approximately 2 mm diameter at the sample, which was contained in a 1 cm quartz cuvette. The contents of the cuvette was stirred continuously during the period of photolysis. The photon flux was determined from the optical power, which was measured using a Thorlabs S120VC photodiode connected to a PM100USB optical power and energy meter. All photolyses for quantum yield determinations were performed in THF with 1% triethylamine added to inhibit thermal decomposition. The initial concentrations were chosen to have an absorbance near 1.5 at the irradiation wavelength, and the photolysis time was typically chosen to result in a decrease in absorbance of approximately 0.2 absorbance units, ensuring that the fraction of incident radiation absorbed is nearly constant over the course of photolysis. UV–vis spectra were recorded at 20.0 °C before and after photolysis. Concentration changes were determined by measuring the absorbance change at the LMCT absorbance maximum. Exhaustive photolysis showed that the decomposition products do not absorb at the wavelength of the LMCT band, and thus no correction for product absorbance was necessary.

Photochemical Decomposition of $\text{Cp}_2\text{Ti}(\text{C}_2\text{DMA})_2$. Samples of the complex (30 mg) in anhydrous THF (12 mL) were degassed with three freeze–pump–thaw cycles and then irradiated using a Rayonet RPR-100 photochemical reactor equipped with eight RPR-5750 bulbs. Organic products were purified by column chromatography (SiO_2 and CH_2Cl_2).

RESULTS AND DISCUSSION

Structural Characterization. All three complexes investigated herein were previously reported without X-ray diffraction data.²⁷ Previous attempts to grow crystals were

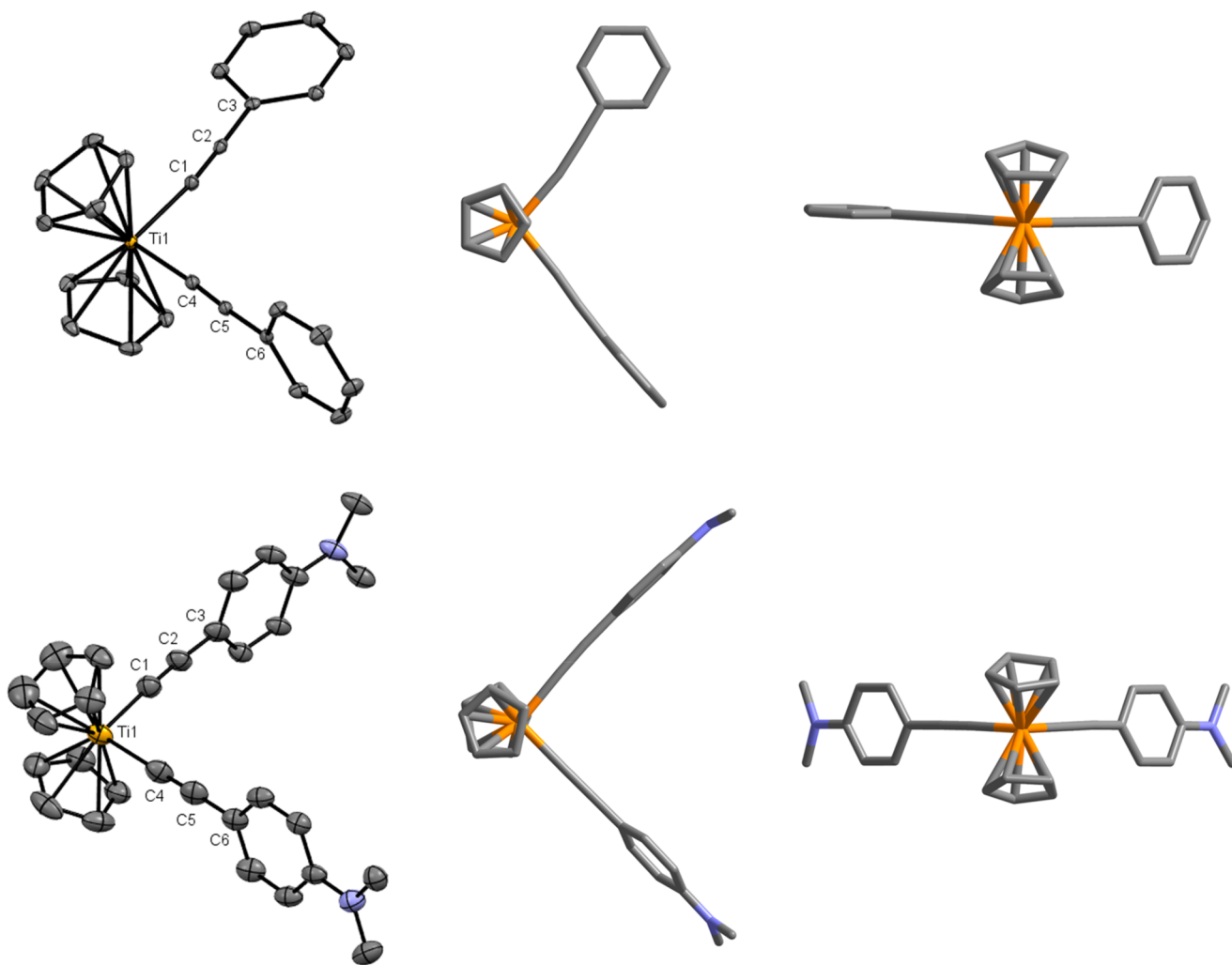


Figure 3. Top row: Structure of $\text{Cp}_2\text{Ti}(\text{C}_2\text{Ph})_2$ shown as 50% probability ellipsoids along with tube diagrams showing the 90/0 conformation for the aryl rings. Bottom row: Structure of $\text{Cp}_2\text{Ti}(\text{C}_2\text{DMA})_2$ shown as 30% probability ellipsoids along with tube diagrams showing the nearly 90/90 conformation for the aryl rings. H atoms are omitted for clarity.

hampered by poor long-term thermal stability in solution. The fact that a similar complex with 2-ethynylpyridine ligands in place of the ethynylbenzene ligands is much more stable in solution⁵¹ suggested that a base (i.e., the pyridine ligand) improved the solution stability. Indeed, the addition of 1–5% triethylamine resulted in weeks-long stability in solution. Thus, crystal growth, spectroscopic measurements, and quantum yield measurements were performed in the presence of triethylamine to avoid thermal decomposition. Despite good long-term stability, conditions for growing single crystals of $\text{Cp}_2\text{Ti}(\text{C}_2\text{TPA})_2$ were not found.

The structures for $\text{Cp}_2\text{Ti}(\text{C}_2\text{Ph})_2$ (Figure 3, top row, Table 1, and Table S1 and Figure S1) and $\text{Cp}_2\text{Ti}(\text{C}_2\text{DMA})_2$ (Figure 3, bottom row, Table 1, and Table S1 and Figure S2) are reported herein. In the solid-state structure of $\text{Cp}_2\text{Ti}(\text{C}_2\text{Ph})_2$, the Ph ring planes are rigidly normal to one another, as imposed by a mirror plane in the molecule. That is, one Ph ring is in the plane defined by the C1–Ti–C4 unit, and the other is oriented perpendicular to that plane. It is useful in this context to define the rotation of each Ph ring relative to this C1–Ti–C4 plane, identifying each aryl ring with its angle relative to this plane. Thus, this structure is rigidly 0/90. The intermolecular interactions are dominated by H $\cdots\pi$ inter-

Table 1. Key Geometric Parameters^a

bond	$\text{Cp}_2\text{Ti}(\text{C}_2\text{Ph})_2$	$\text{Cp}_2\text{Ti}(\text{C}_2\text{DMA})_2^b$
Ti–C1	2.108(3)	2.081(6), 2.088(6)
Ti–C4	2.096(3)	2.111(7), 2.096(7)
C1–C2	1.222(4)	1.215(7), 1.227(8)
C4–C5	1.222(4)	1.214(8), 1.236(8)
C1–Ti–C4	100.68(12)	96.3(2), 94.2(2) ^c
Ar1 dihedral angle ^c	0.0	86.0, 83.8
Ar2 dihedral angle ^c	90.0	78.5, 78.9

^aAll bond lengths in angstroms and angles in degrees. ^bThere are two unique molecules in the asymmetric unit for $\text{Cp}_2\text{Ti}(\text{C}_2\text{DMA})_2$. The comparable parameters for each molecule are listed. ^cThe dihedral angles are defined as those between the C1–Ti–C4 plane and each aryl plane. Ar1 is the aryl linked to the C1 \equiv C2 alkyne, and Ar2 is the aryl linked to the C4 \equiv C5 alkyne.

actions (Figure S1). The corresponding zirconocene complex, $\text{Cp}_2\text{Zr}(\text{C}_2\text{Ph})_2$, has an identical 0/90 structure in the solid state.⁵² It is worth noting that a very similar complex with a trimethylsilyl-substituted Cp ring, $^{\text{TMS}}\text{Cp}_2\text{Ti}(\text{C}_2\text{Ph})_2$, crystallizes in a conformation with the Ph rings face-to-face (very nearly 90/90).⁵³ Thus, the energy difference between these rotamers might be very small and the Ph ring conformation in

the solid-state driven by crystal packing considerations. In contrast, for $\text{Cp}_2\text{Ti}(\text{C}_2\text{DMA})_2$, the aryl rings are nearly face-to-face (90/90) with intermolecular interactions also involving π stacking (Figure S2) in addition to $\text{H}\cdots\pi$ interactions. The intermolecular interactions for the two DMA units within a single complex are different because the two aryl rings are inequivalent in the solid-state structure and there are two unique complexes in the asymmetric unit. Lastly, The C1–Ti–C4 bite angle in $\text{Cp}_2\text{Ti}(\text{C}_2\text{Ph})_2$ is larger than the corresponding angle in $\text{Cp}_2\text{Ti}(\text{C}_2\text{DMA})_2$.

Photophysics. The UV–vis spectra of the three complexes investigated herein have been previously reported in CH_2Cl_2 . The lowest-energy transitions have been ascribed to a LMCT transition from the alkynylarylamine to Ti^{IV} .²⁷ For simplicity of the computational solvent model choice, the UV–vis spectra (Figure 4 and Table 2) are reported in THF (dielectric

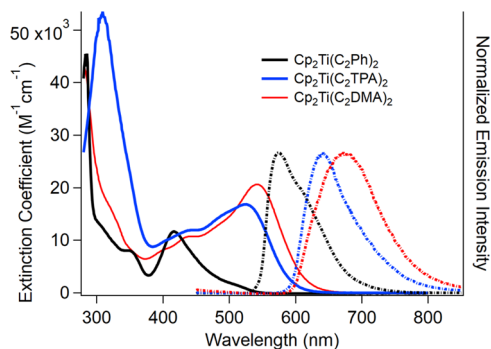


Figure 4. UV–vis and normalized emission spectra of $\text{Cp}_2\text{Ti}(\text{C}_2\text{Ph})_2$, $\text{Cp}_2\text{Ti}(\text{C}_2\text{DMA})_2$, and $\text{Cp}_2\text{Ti}(\text{C}_2\text{TPA})_2$. UV–vis spectra are in THF at 20 °C. Emission spectra are in 2-methyltetrahydrofuran (1% triethylamine, v/v) glass at 77 K.

Table 2. Photophysical and Photochemical Data

complex	λ_{abs}^a	λ_{em}^b	ϕ_{decomp} in air (Ar) ^c
$\text{Cp}_2\text{Ti}(\text{C}_2\text{DMA})_2$	540	672	0.25 (0.25)
$\text{Cp}_2\text{Ti}(\text{C}_2\text{TPA})_2$	525	642	0.40 (0.42)
$\text{Cp}_2\text{Ti}(\text{C}_2\text{Ph})_2$	417	575	0.99 (0.65)

^aLowest-energy absorption maximum (nm) in THF at 20 °C.

^bEmission maximum in 2-methyltetrahydrofuran at 77 K. $\lambda_{\text{ex}} = 400$ nm.

^cQuantum yield for photodecomposition in a room-temperature THF solution upon excitation into the lowest-energy absorption band.

constant = 7.58) for consistency with emission spectra, which were recorded in 2-methyltetrahydrofuran glass (dielectric constant = 6.97). The UV–vis spectra are slightly blue-shifted (3–14 nm) in THF versus CH_2Cl_2 . This is consistent with the investigation of the solvatochromism of the CT-to- Ti^{IV} absorption bands in $^R\text{Cp}_2\text{Ti}(\text{C}_2\text{Fc})_2$ complexes. In that study, the solvent polarizability dominated the solvatochromism, with the CT absorption band energy decreasing with increased solvent polarizability (CH_2Cl_2 is more polarizable than THF).⁵⁴ Not surprisingly, this suggests a greater degree of electron delocalization in the excited state than the ground state.⁵⁵ TDDFT confirms that the lowest-energy absorption for all three complexes is to an excited state of the same ¹LMCT electronic nature (vide infra).

Upon excitation into this ¹LMCT band, all complexes are brightly emissive in a 2-methyltetrahydrofuran glass at 77 K (Figure 4 and Table 2) and weakly emissive at room temperature as a microcrystalline solid. The room-temperature

solid spectra are red-shifted from those recorded in a 77 K glass (Figure S3). Excitation spectra closely match the UV–vis spectra, indicating that emission is not due to an impurity (Figure S4). Emission from Cp_2TiX_2 complexes ($X = \text{F}^-$, Cl^- , Br^- , SCN^-) at 77 K has been observed previously. In the case of $X = \text{halide}$, emission was ascribed to a Cp-to-Ti LMCT triplet excited state, although the authors also considered emission from an X-to-Ti LMCT triplet excited state.⁵⁶ Emission from $\text{Cp}_2\text{Ti}(\text{SCN})_2$ was ascribed to a SCN-to-Ti LMCT triplet excited state based on the TDDFT data.⁵⁷ For the arylalkynylamine complexes investigated herein, prior evidence that the lowest-energy absorption generates an LMCT excited state and further quantum-chemical calculations (vide infra) suggest that emission is from an arylalkynylamine-to- Ti^{IV} ³LMCT state. The significant red shift (3000–4000 cm^{-1}) of the emission relative to the absorption is consistent with emission following intersystem crossing (ISC) to a lower-energy triplet, although the extent to which this ISC is quantitative is unclear given the lack of atoms with significant spin–orbit coupling constants.⁵⁸

Photochemistry. Previous reports indicate that the complexes investigated herein are not photostable.^{26,27} For example, photolysis of $\text{Cp}_2\text{Ti}(\text{C}_2\text{Ph})_2$ in THF, benzene, or toluene results in an enyne (Figure 5, R = H). The proposed

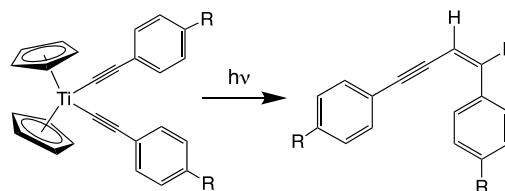


Figure 5. Organic photodecomposition product of arylalkynyltitanocenes.

mechanism involves the reductive elimination of a diyne followed by reduction of the diyne to the enyne by the resulting titanocene.²⁶ The so-called “titanocene” has been demonstrated to have a dihydride structure, where the hydrides come from the coupling of two Cp rings into a fulvalene structure,⁵⁹ and this titanocene has been demonstrated to be a good reducing agent.⁶⁰ The fact that photolysis in a deuterated solvent did not result in deuterium incorporation into the enyne product supported this conclusion.²⁶ Herein, we report that photolysis of $\text{Cp}_2\text{Ti}(\text{C}_2\text{DMA})_2$ under an inert atmosphere also results in an enyne as the dominant organic photoproduct (Figure 5, R = NMe_2), consistent with prior results for $\text{Cp}_2\text{Ti}(\text{C}_2\text{Ph})_2$ photolysis. The enyne product is predominantly cis with a cis-to-trans ratio of 4:1, as demonstrated by a comparison of the ¹H NMR spectrum with those of authentic samples. The enyne is typically contaminated with a small quantity of the corresponding diyne, which further supports the intermediacy of the diyne in the formation of the enyne (Figure S5). Such a C–C coupling reaction may proceed through the intermediacy of a titanacyclopentene.^{61,62} We also report here the quantum yields for photodecomposition (Table 2 and Figure S6) for all three complexes, which range from 0.25 to nearly 1. Within experimental error, the quantum yields for photodecomposition of $\text{Cp}_2\text{Ti}(\text{C}_2\text{DMA})_2$ and $\text{Cp}_2\text{Ti}(\text{C}_2\text{TPA})_2$ are not affected by the presence of oxygen. However, the quantum yield for decomposition of $\text{Cp}_2\text{Ti}(\text{C}_2\text{Ph})_2$ increases by a factor of approximately 1.5 in the presence of air.

Table 3. Comparison of DFT-Predicted and Experimental Bond Metrics^a for Cp₂Ti(C₂DMA)₂

bond	X-ray	ω B97XD/6-311+G(d)		CAM-B3LYP/6-311+G(d)		B3PW91/6-311+G(d)		B3LYP/6-311+G(d)		MN15/LANL2DZ	
		DFT	Δ^b	DFT	Δ^b	DFT	Δ^b	DFT	Δ^b	DFT	Δ^b
C–C _{Cp} ^c	1.373	1.412	0.039	1.410	0.037	1.414	0.041	1.416	0.043	1.430	0.057
Ti–C _{Cp} ^d	2.358	2.372	0.014	2.383	0.025	2.387	0.029	2.418	0.060	2.387	0.029
Ti–C ^e	2.094	2.087	–0.007	2.085	–0.009	2.074	–0.020	2.084	–0.010	2.045	–0.049
C≡C ^e	1.223	1.223	0.000	1.220	–0.003	1.232	0.009	1.230	0.007	1.249	0.026
C–Ti–C	95.3	95.52	0.2	95.57	0.3	95.65	0.4	95.79	0.5	96.12	0.8

^aAll bond lengths are given in angstroms and bond angles in degrees. Metrics for the crystal data are averages of the two unique molecules in the asymmetric unit. All computational models were run with scrf (solvent = thf). ^b Δ is the difference between the calculated structure (DFT) and X-ray structure. ^cThe C–C bond lengths of the Cp rings were averaged. ^dThe bond lengths between the Ti and the C atoms on the Cp rings were averaged. ^eThe ethynyl dimethylaniline ligands are crystallographically inequivalent. Thus, the bond lengths were averaged for comparison with the calculated structure.

Computational Modeling. Computational Benchmarking. Previously reported computational modeling of the spectra of these titanocenes was performed with ω B97XD/def2-TZV for the geometry optimization and B3PW91/6-311G(d,p) for the TDDFT.²⁷ This model had been chosen based on its reasonable prediction of the lowest-energy absorption band for complexes of the type ^RCp₂Ti(C₂Fc)₂.²⁶ Although this model did a reasonable job of predicting the lowest-energy absorption band for the ethynylarylamine complexes investigated herein, the predicted energies for Cp₂Ti(C₂DMA)₂ and Cp₂Ti(C₂TPA)₂ were reversed versus experiment. Thus, we have undertaken an extensive benchmarking effort using the structural data reported herein, as well as both the absorption and emission energies. Because all spectroscopic data reported herein are recorded in THF or 2-methyltetrahydrofuran, all calculations employ a Tomasi polarizable continuum model assigned the dielectric constant for THF.⁶³

The structure of Cp₂Ti(C₂DMA)₂ was optimized using a range of functionals and basis sets. Functionals chosen because of recent success in predicting the structures of a range of titanocenes include B3LYP,⁶⁴ B3PW91,^{28,29} M06,⁶⁵ and M06-L.⁶⁶ Because of interest in the CT transitions in these complexes, the range-separated functionals ω B97XD and CAM-B3LYP were also investigated. ω B97XD is also a dispersion-corrected functional and is known to more accurately predict structure. We also investigated the addition of a Grimme's dispersion correction.⁶⁷ A range of basis sets was investigated, including double- ζ basis sets, 6-31G(d) and LANL2DZ, and triple- ζ basis sets, 6-311+G(d) and def2-TZV. All models predicted the bond lengths within the dimethylaniline portion of the complex with low deviations (<0.015 Å) relative to the crystal structure; thus, models were analyzed with respect to the bond lengths and angles surrounding the Ti. Structures calculated with the 6-311+G(d) basis set were the most faithful in their agreement with the crystal structure and were most accurate when paired with ω B97XD and CAM-B3LYP (Table 3). The addition of dispersion corrections did not appear to improve the models.

Next, functionals for TDDFT were screened by first optimizing both Cp₂Ti(C₂DMA)₂ and Cp₂Ti(C₂TPA)₂ using ω B97XD/6-311+G(d) and then performing TDDFT using a series of functionals paired with the 6-31G(d) basis set. In addition to the functionals screened for geometry optimization, several more from the Minnesota family of functionals were added because this class of functionals is highly parametrized to obtain a balanced description for both main-group and

transition-metal systems and they have been significantly benchmarked.⁶⁸ These include M05, M06, M11, SOGGA11, MN12SX, N12SX, and MN15. Lastly, B97D3, an additional dispersion-corrected functional, was added. The predicted lowest-energy singlet transitions for six of the TDDFT models had errors of more than 100 nm versus the experimental absorbance and were eliminated from further consideration (Table S2). The remaining seven functionals were paired with a different double- ζ basis set, LANL2DZ. Although all models gave reasonable predictions of the energy of the lowest-energy transitions, MN15 was the only model that correctly predicted that the lowest-energy transition of Cp₂Ti(C₂DMA)₂ is at a longer wavelength than that of Cp₂Ti(C₂TPA)₂ (Table S3). Next, MN15 was paired with two more sophisticated triple- ζ basis sets [6-311+G(d) and def2-TZV] for a comparison with those already run. The less computationally intensive MN15/LANL2DZ combination clearly models the lowest-energy transition the most faithfully (Table 4).

Table 4. Lowest-Energy Singlet Transitions Predicted for Cp₂Ti(C₂DMA)₂ and Cp₂Ti(C₂TPA)₂ Using the MN15 Functional^a

	exp ^b	LANL2DZ	6-311+G(d)	def2-TZV	6-31G(d)
Cp ₂ Ti(C ₂ DMA) ₂	540	523	485	487	486
Cp ₂ Ti(C ₂ TPA) ₂	525	518	486	484	487

^aAll TDDFT models were run with ω B97XD/6-311+G(d) geometry in THF. All values reported are in nanometers. The wavelengths reported for the TDDFT are the lowest-energy singlet transitions.

^bLowest-energy absorbance peak in THF.

Lastly, the effect of the geometry on the TDDFT predictions was investigated. In this final iteration, all three complexes were included in the benchmarking and the lowest-energy vertical singlet and triplet transitions were compared to the room-temperature absorption and 77 K emission data (Table 5). TDDFT using MN15/LANL2DZ was performed starting with the four models for geometry optimization that were determined to most closely match the experimental structure. In addition, a fifth geometry optimization model was chosen (MN15/LANL2DZ) because it is common to perform TDDFT and geometry optimization using the same model.

MN15/LANL2DZ//MN15/LANL2DZ (TDDFT//opt) modeled the absorption data with the greatest fidelity but only slightly more accurately than MN15/LANL2DZ//B3LYP/6-311+G(d). Despite the fact that vertical S₀-to-T₁ transitions should slightly overestimate the T₁-to-S₀ emission

Table 5. Lowest-Energy Singlet and Triplet Transitions Predicted from TDDFT Using MN15/LANL2DZ with Various Optimized Geometries^a

	exp ^b	MN15/LANL2DZ	B3LYP/6-311+G(d)	ω B97XD/6-311+G(d)	CAM-B3LYP/6-311+G(d)	B3PW91/6-311+G(d)
Lowest-Energy Singlet						
Cp ₂ Ti(C ₂ DMA) ₂	540	537	542	523	524	538
Cp ₂ Ti(C ₂ TPA) ₂	525	531	534	518	518	539
Cp ₂ Ti(C ₂ Ph) ₂ ^c	417	423	426	416	416	421
Lowest-Energy Triplet						
Cp ₂ Ti(C ₂ DMA) ₂	672	680	670	638	671	668
Cp ₂ Ti(C ₂ TPA) ₂	642	653	641	614	612	640
Cp ₂ Ti(C ₂ Ph) ₂ ^c	575	578	569	555	554	563

^aAll TDDFT models included THF. All values reported are in nanometers. ^bThe wavelengths reported are for the lowest-energy absorbance peak in THF and the 77 K emission peak in 2-methyltetrahydrofuran. ^cThe Cp₂Ti(C₂Ph)₂ structure was optimized in the 90/0 conformation to be consistent with X-ray crystallographic data. The TDDFT-calculated singlet transition given here is the lowest-energy singlet with significant oscillator strength.

energies, depending on the magnitude of the Stokes shift, TDDFT-determined S₀-to-T₁ transitions have been used to estimate the observed triplet 0–0 bands with good accuracy, particularly where the matrixes provide a rigid environment for the emitter molecule.^{69,70} This is due to the rigid medium enforcing an excited-state structure very close to that of the S₀ minimum.⁷¹ The reported experimental emission wavelengths are the maxima at 77 K, well below the glass transition temperature for the 2-methyltetrahydrofuran solvent, and are accurately modeled by the S₀-to-T₁ transitions (Table 5). Emission energies are often calculated using Δ SCF methods.^{72,73} Predictably, using the relaxed T₁ geometry in these calculations does not accurately model the emission energies under these conditions, whereas Δ SCF calculations on the S₀ geometry result in much better agreement (Figure S7 and Table S4). Lastly, it is worth noting that, because these emission bands are not resolved, the 0–0 transitions may be at slightly higher energies than the experimental 77 K maxima.

For all complexes, the highest occupied molecular orbital (HOMO) is dominated by the arylalkynyl ligand and the lowest unoccupied molecular orbital (LUMO) is dominated by d_{2⁻²-y²}, with the C₂ axis being defined as the z axis (Figure 6 and Charts S1–S3). For both Cp₂Ti(C₂Ph)₂ and Cp₂Ti(C₂DMA)₂, LUMO through LUMO+4 involve the complete set of five d orbitals, whereas for Cp₂Ti(C₂TPA)₂, LUMO+4 is ligand-dominated. These orbitals do not change meaningfully when calculated using ω B97XD/6-311+G(d) instead of MN15/LANL2DZ. Qualitatively similar orbital orderings have been observed for Cp₂Ti(SCN)₂.⁵⁷ The lowest-energy singlets and triplets are dominated by a HOMO-to-LUMO transition (Charts S1–S3). This suggests that the lowest-energy visible absorption band involves promotion to a ¹LMCT and that the emission originates from the ³LMCT state.

Contribution of Rotational Isomerism. It is noteworthy that, for the optimized structures for all three complexes, the two aryl rings attached to the alkyne linkers are face-to-face (approximately 90/90). For both Cp₂Ti(C₂DMA)₂ and Cp₂Ti(C₂TPA)₂, the TDDFT-predicted electronic transitions from the optimized structures closely match the experimental spectrum, particularly at longer wavelengths (Figure 7). This is not the case for Cp₂Ti(C₂Ph)₂, where neither the energy nor the band shape are well represented by the TDDFT-predicted spectrum from the optimized structure (86/86). In particular, the experimental absorption spectrum is blue-shifted with a substantial red tail (Figure 8). Optimizing the structure with a

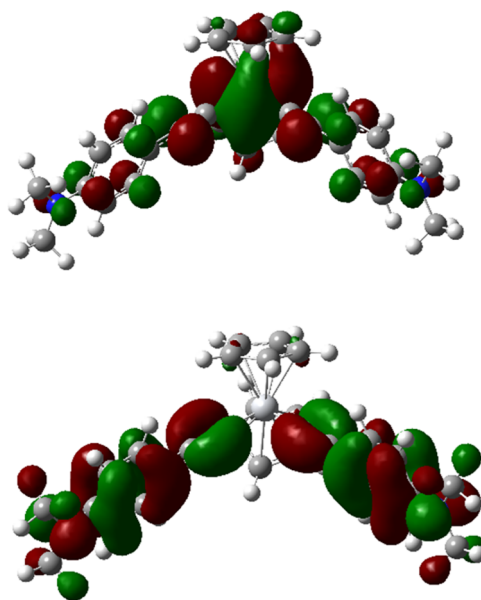


Figure 6. HOMO (bottom) and LUMO (top) for Cp₂Ti(C₂DMA)₂ at the MN15/LANL2DZ level of theory. Additional frontier orbitals for this complex and for Cp₂Ti(C₂Ph)₂ and Cp₂Ti(C₂TPA)₂ appear in the Supporting Information. A default isovalue of 0.02 is used for all surfaces.

dihedral angle constraint that imposes the 90/0 structure observed in the solid state more accurately predicts the absorption maximum but fails to model the red tail in the experimental spectrum. This suggests that the room-temperature solution spectrum may be composed of a collection of conformers that result from free rotation of the phenyl rings.

To investigate this phenomenon, an electronic energy scan with 15° increments of each phenyl ring was performed at the MN15/LANL2DZ level of theory. The angle between each phenyl ring and the C1–Ti–C4 plane was constrained and the geometry optimized for each rotamer. This demonstrated a maximum very near 0/0. However, the potential energy surface was quite flat (Figure 9) with an electronic energy difference between the minimum and maximum of less than 1.3 kcal/mol, suggesting that free rotation in solution is likely. This is also consistent with the result (vide supra) that Cp₂Ti(C₂Ph)₂ crystallizes in the 90/0 conformation, whereas the trimethylsilyl-substituted ^{TMS}Cp₂Ti(C₂Ph)₂ complex crystallizes in nearly a 90/90 conformation, i.e., that the small rotamer

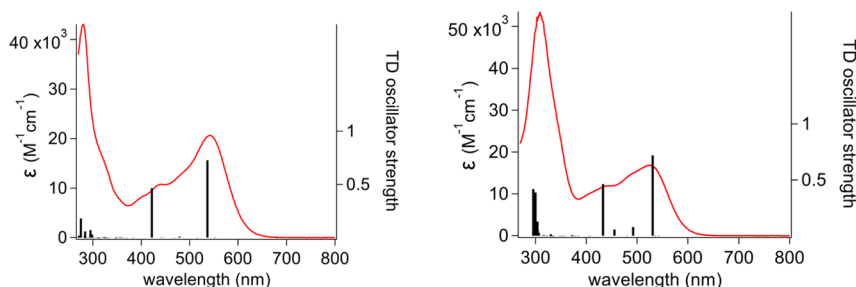


Figure 7. Overlay of UV-vis spectrum (THF) and TDDFT (MN15/LANL2DZ//MN15/LANL2DZ)-predicted vertical transitions for $\text{Cp}_2\text{Ti}(\text{C}_2\text{DMA})_2$ (left) and $\text{Cp}_2\text{Ti}(\text{C}_2\text{TPA})_2$ (right).

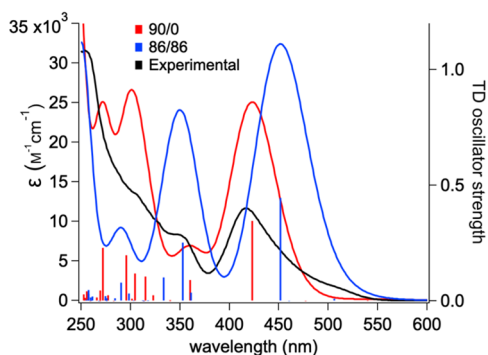


Figure 8. Comparison of the experimental UV-vis spectrum of $\text{Cp}_2\text{Ti}(\text{C}_2\text{Ph})_2$ in THF (black) with that predicted from TDDFT (MN15/LANL2DZ//MN15/LANL2DZ) on the 86/86 (blue) and 90/0 (red) rotamers. For spectral prediction, a half-width at half-maximum of 1500 cm^{-1} was used.

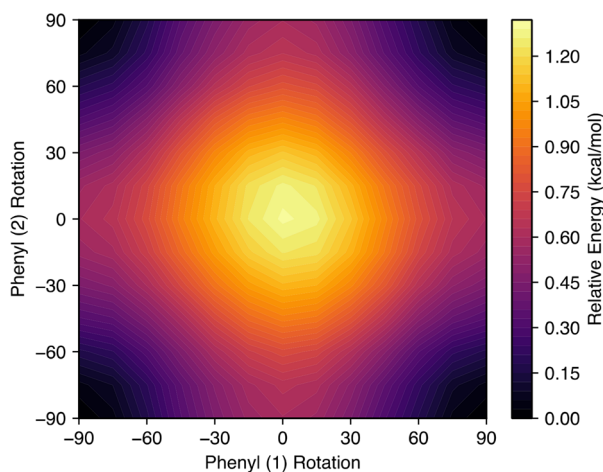


Figure 9. Electronic energy contour plot for $\text{Cp}_2\text{Ti}(\text{C}_2\text{Ph})_2$ that scans a full 180° rotation of each phenyl ring. 0° is defined as the phenyl ring being in the $\text{C}1\text{-Ti-C}4$ plane.

energy differences lead to solid-state structures dominated by crystal packing energetics.

To approximate a UV-vis spectrum that is comprised of all rotamers, TDDFT was performed on five rotamers chosen to represent the conformational space, and their predicted UV-vis spectra were averaged. The rotamers chosen to represent the conformational space were 90/90, 45/45, 0/0, 45/−45, and 90/0 (Figure 10). Small deviations (5°) were determined to result in relatively small shifts of the predicted transitions; thus, each rotamer is a reasonable representation of geometrically similar rotamers, and the 45° steps are warranted. For

each structure that lacks a C_2 axis, two different orientations will result in equivalent predicted transitions (e.g., 45/−45 and −45/45 will give the same transitions). Thus, the contributions from 45/−45 and 90/0 have been doubled in the average (Figure 10). Weighted Boltzmann averaging was not taken into account due to the energy differences being smaller than the typical uncertainties in DFT-determined electronic energies. It is notable that a relatively small but inclusive sampling of the conformational space results in remarkably good agreement between the experimental and theoretically predicted spectra, particularly in the low-energy region. The 90/0 rotamer dominates the low-energy absorption maximum, and the 90/90 and 45/−45 rotamers are largely responsible for the red tail. In a related example of tungsten(0) arylisocyanides, $\text{W}(\text{CNAr})_6$, two distinct conformers were evident in the solution-phase UV-vis spectra, namely, where trans aryl rings were either mutually perpendicular or parallel.⁷⁴ In that case, only two conformers were necessary to describe the spectrum. To our knowledge, the system herein is the first example of modeling a UV-vis spectrum where freely rotating conformers contribute.

It is noteworthy that, for $\text{Cp}_2\text{Ti}(\text{C}_2\text{DMA})_2$ and $\text{Cp}_2\text{Ti}(\text{C}_2\text{TPA})_2$, it was unnecessary to include rotamer contributions in order to obtain good agreement between the predicted and experimental UV-vis. Although a full rotamer scan of these complexes was not performed, an analysis of the minimum (90/90) and maximum (0/0) energy conformations for $\text{Cp}_2\text{Ti}(\text{C}_2\text{DMA})_2$ demonstrates a 3-fold larger energy difference than that for $\text{Cp}_2\text{Ti}(\text{C}_2\text{Ph})_2$ (4.0 vs 1.3 kcal/mol). We hypothesize that such rotamers are not as important for $\text{Cp}_2\text{Ti}(\text{C}_2\text{TPA})_2$ and $\text{Cp}_2\text{Ti}(\text{C}_2\text{DMA})_2$ because conjugation involving the lone pair on the N atoms results in a structure with cumulene-type character, $\text{Ti}=\text{C}=\text{C}=\text{C}_{\text{Aryl}}$, that restricts such rotation. The MN15/LANL2DZ-optimized [using $\text{Cp}_2\text{Ti}(\text{C}_2\text{Ph})_2$ in the 90/0 conformation] and crystal structures are both consistent with this hypothesis. Namely, the calculated and experimental Ti–C bonds are approximately 0.01 Å shorter in $\text{Cp}_2\text{Ti}(\text{C}_2\text{DMA})_2$ than $\text{Cp}_2\text{Ti}(\text{C}_2\text{Ph})_2$. Consistent with this, the C–C_{Aryl} bond is shorter for $\text{Cp}_2\text{Ti}(\text{C}_2\text{DMA})_2$ than for $\text{Cp}_2\text{Ti}(\text{C}_2\text{Ph})_2$ (by 0.006 Å for DFT and 0.003 Å in the solid state). Likewise, the C≡C bond is slightly longer for $\text{Cp}_2\text{Ti}(\text{C}_2\text{DMA})_2$ than for $\text{Cp}_2\text{Ti}(\text{C}_2\text{Ph})_2$, but the effect is more subtle (0.003 Å for DFT and 0.001 Å in the solid state). A similar type cumulene structure has been proposed to contribute to bonding with an organic donor–acceptor system with *N,N*-dimethylaniline linked to an organic acceptor through an ethynyl bridge.⁷⁵

Exploring the Triplet Geometry. Because the observed photodecomposition is likely to occur out of the $^3\text{LMCT}$ state, we investigated optimization of the complexes in their lowest-

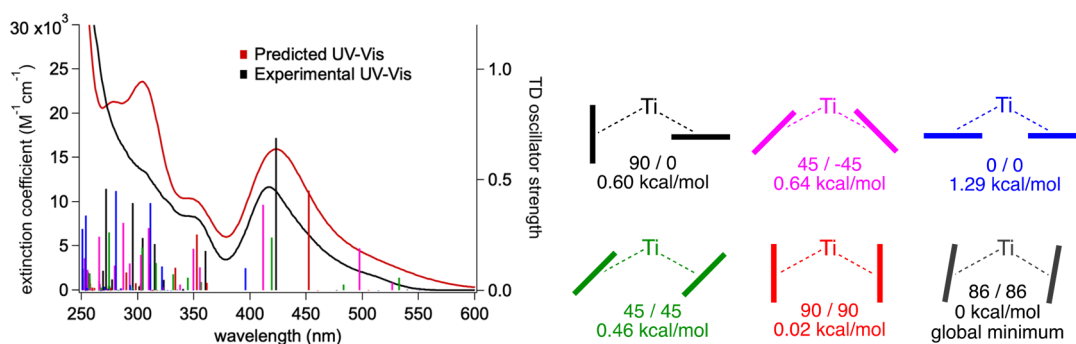


Figure 10. Left: Comparison of the experimental UV–vis spectrum in THF (black) with that predicted from an average of rotamers (red). For spectral prediction, a half-width at half-maximum of 1500 cm⁻¹ was used. The vertical transitions and oscillator strengths are represented by vertical bars. Right: Rotamers represented in the average spectrum along with energy relative to the global minimum (86/86). The colors represent the predicted vertical transition bars in the UV–vis spectrum.

energy triplet states. Using MN15/LANL2DZ for the triplet optimizations, all three complexes show cleavage of the Ti–C_{alkynyl} bonds and the formation of a C–C bond between the two alkyne fragments (Figure S8). This is consistent with the known room-temperature photolysis products but inconsistent with the fact that these complexes are emissive at 77 K and show no sign of decomposition at that temperature. After attempting several models, B3LYP/def2-TZV triplet optimizations maintained structural integrity for Cp₂Ti(C₂DMA)₂ and Cp₂Ti(C₂TPA)₂, i.e., did not result in Ti–C bond cleavage. Instead, there was a compression of the C1–Ti–C4 bond angle by approximately 25°, thus bringing the C atoms attached to the Ti atom into closer proximity (Figure S9). This is consistent with a reaction trajectory that forms a new C–C bond, in agreement with the known photolysis products (Figure 5). For Cp₂Ti(C₂Ph)₂, all models investigated resulted in Ti–C bond cleavage upon optimization of the lowest-energy triplet. Additionally, attempts at triplet optimization for Cp₂Ti(C₂Ph)₂ by replacing NMe₂ with H in the T₁-optimized structure of Cp₂Ti(C₂DMA)₂ also resulted in Ti–C bond cleavage.

The fact that such distortions are consistent with the photodecomposition products suggests that rigidifying the complex against a C1–Ti–C4 bond angle compression may stabilize the complex to photolysis. In this regard, it is interesting that related arylalkynyltitanocenes with pentamethylcyclopentadienyl (Cp*) ligands are photosensitive but have been reported to be photostable upon coordination of Cu^I between the alkynes or of Pd^{II} between the pyridine N atoms (Figure 11).⁵¹ No investigation of the mechanism of photostabilization has been reported. The results herein suggest that the increased photostability may result from Cu^I preventing compression of the C1–C4 distance, thus inhibiting C1–C4 bond formation. Research is ongoing to

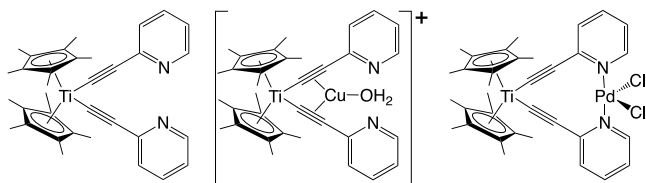


Figure 11. Cp*₂Ti complexes with 2-ethynylpyridine ligands. The complex on the left is photosensitive, whereas the complexes rigidified with Cu^I or Pd^{II} are photostable.

investigate the mechanism of photostabilization as well as whether such photostabilization can be exploited.

CONCLUSIONS

Complexes with LMCT excited states involving d⁰ metals have the possibility of strongly emissive, long-lived excited states due to a lack of ³MC states. Herein, the photochemistry and photophysics of a series of titanocenes with substituted arylalkynyl ligands were investigated with the help of computational modeling. All complexes show high molar-absorptivity transitions in the visible region and are brightly emissive at 77 K. A range of computational methods were investigated and benchmarked against both the absorption and emission spectra. Proper modeling of the absorption spectrum for Cp₂Ti(C₂Ph)₂ required an accounting for rotational isomerism. The computational models demonstrate that the lowest-energy absorption and emission involve ¹LMCT and ³LMCT states, respectively. At room temperature, all complexes undergo photodegradation with quantum yields between 0.25 and 0.99. Kasha's rule states that emission (and, by extension, photoreaction) takes place from the lowest-energy state of a given spin multiplicity;⁷⁶ thus, it is likely that the ³LMCT excited state is responsible for both emission and photoreaction. In this regard, it is interesting that the lowest-energy triplet is distorted along a C–Ti–C bond angle compression coordinate that could lead to the observed photoproducts. It is also noteworthy that, at least with the set of complexes investigated herein, there is a clear trend of increased photodecomposition quantum yield with ³LMCT energy. We are presently investigating the degree to which each of these parameters (excited-state energy and excited-state distortion) impact the photostability of the complexes so that photostable complexes with long-lived ³LMCT states can be designed.

ASSOCIATED CONTENT

Supporting Information

The Supporting Information is available free of charge at <https://pubs.acs.org/doi/10.1021/acs.inorgchem.1c02182>.

Crystallographic data for Cp₂Ti(C₂Ph)₂ and Cp₂Ti(C₂DMA)₂, several different orientations and packing arrangements for their structures, excitation and solid-state emission spectra for all complexes, ¹H NMR spectrum of photodecomposition products for Cp₂Ti(C₂DMA)₂, UV–vis spectra before, during, and after

photodecomposition of all complexes, TDDFT benchmarking data with additional functionals and basis sets, emission energies from Δ SCF calculations, frontier molecular orbitals and TDDFT data for lowest-energy singlets and triplets for all complexes, and optimized triplet geometries for all complexes (PDF)

Cartesian coordinates for all structures optimized as singlets at the MN15/LANL2DZ level (XYZ)

Cartesian coordinates for all structures optimized as triplets (XYZ)

Accession Codes

CCDC 2095566 and 2095567 contain the supplementary crystallographic data for this paper. These data can be obtained free of charge via www.ccdc.cam.ac.uk/data_request/cif, or by emailing data_request@ccdc.cam.ac.uk, or by contacting The Cambridge Crystallographic Data Centre, 12 Union Road, Cambridge CB2 1EZ, UK; fax: +44 1223 336033.

AUTHOR INFORMATION

Corresponding Authors

Paul S. Wagenknecht – Department of Chemistry, Furman University, Greenville, South Carolina 29609, United States;

orcid.org/0000-0001-8698-073X;

Email: paul.wagenknecht@furman.edu

George C. Shields – Department of Chemistry, Furman University, Greenville, South Carolina 29609, United States;

orcid.org/0000-0003-1287-8585;

Email: george.shields@furman.edu

Authors

Henry C. London – Department of Chemistry, Furman University, Greenville, South Carolina 29609, United States

Thomas J. Whitemore – Department of Chemistry, Furman University, Greenville, South Carolina 29609, United States

Ariel G. Gale – Department of Chemistry, Furman University, Greenville, South Carolina 29609, United States

Colin D. McMillen – Department of Chemistry, Clemson University, Clemson, South Carolina 29634, United States;

orcid.org/0000-0002-7773-8797

David Y. Pritchett – Department of Chemistry, Furman University, Greenville, South Carolina 29609, United States

Alexis R. Myers – Department of Chemistry, Furman University, Greenville, South Carolina 29609, United States

Hannah D. Thomas – Department of Chemistry, Furman University, Greenville, South Carolina 29609, United States

Complete contact information is available at:

<https://pubs.acs.org/10.1021/acs.inorgchem.1c02182>

Notes

The authors declare no competing financial interest.

ACKNOWLEDGMENTS

This work was supported by the National Science Foundation under Grant CHE-1362516 (to P.S.W.) and through the EPSCoR Program under NSF Award OIA-1655740. T.J.W. acknowledges summer support from the NSF-REU (Grant CHE-1757706). Any opinions, findings and conclusions or recommendations expressed in this material are those of the authors and do not necessarily reflect those of the National Science Foundation. G.C.S. acknowledges Research Corporation for Science Advancement Cottrell Instrumentation Supplements Award 27446. A.G.G. acknowledges support

through the Arnold and Mabel Beckman Foundation Beckman Scholars Award. The authors acknowledge technical assistance from Togo Odbadrakh.

REFERENCES

- (1) Ashford, D. L.; Gish, M. K.; Vannucci, A. K.; Brennaman, M. K.; Templeton, J. L.; Papanikolas, J. M.; Meyer, T. J. Molecular Chromophore-Catalyst Assemblies for Solar Fuel Applications. *Chem. Rev.* **2015**, *115* (23), 13006–13049.
- (2) Morseth, Z. A.; Wang, L.; Puodziukynaitė, E.; Leem, G.; Gilligan, A. T.; Meyer, T. J.; Schanze, K. S.; Reynolds, J. R.; Papanikolas, J. M. Ultrafast Dynamics in Multifunctional Ru(II)-Loaded Polymers for Solar Energy Conversion. *Acc. Chem. Res.* **2015**, *48* (3), 818–827.
- (3) Ji, J.-M.; Zhou, H.; Kim, H. K. Rational design criteria for D- & A structured organic and porphyrin sensitizers for highly efficient dye-sensitized solar cells. *J. Mater. Chem. A* **2018**, *6* (30), 14518–14545.
- (4) Twilton, J.; Le, C.; Zhang, P.; Shaw, M. H.; Evans, R. W.; MacMillan, D. W. C. The merger of transition metal and photocatalysis. *Nature Reviews Chemistry* **2017**, *1*, 0052.
- (5) Prier, C. K.; Rankic, D. A.; MacMillan, D. W. C. Visible Light Photoredox Catalysis with Transition Metal Complexes: Applications in Organic Synthesis. *Chem. Rev.* **2013**, *113* (7), 5322–5363.
- (6) Castellano, F. N. Altering Molecular Photophysics by Merging Organic and Inorganic Chromophores. *Acc. Chem. Res.* **2015**, *48* (3), 828–839.
- (7) Ko, C.-C.; Yam, V. W.-W. Coordination Compounds with Photochromic Ligands: Ready Tunability and Visible Light-Sensitized Photochromism. *Acc. Chem. Res.* **2018**, *51* (1), 149–159.
- (8) Whitemore, T. J.; Millet, A.; Sayre, H. J.; Xue, C.; Dolinar, B. S.; White, E. G.; Dunbar, K. R.; Turro, C. Tunable Rh2(II,II) Light Absorbers as Excited-State Electron Donors and Acceptors Accessible with Red/Near-Infrared Irradiation. *J. Am. Chem. Soc.* **2018**, *140*, 5161–5170.
- (9) Wagenknecht, P. S.; Ford, P. C. Metal Centered Ligand Field Excited States: Their Roles in the Design and Performance of Transition Metal Based Photochemical Molecular Devices. *Coord. Chem. Rev.* **2011**, *255* (5), 591–616.
- (10) Glaser, F.; Wenger, O. S. Recent progress in the development of transition-metal based photoredox catalysts. *Coord. Chem. Rev.* **2020**, *405*, 213129.
- (11) McCusker, J. K. Electronic structure in the transition metal block and its implications for light harvesting. *Science* **2019**, *363*, 484–488.
- (12) Ravetz, B. D.; Wang, J. Y.; Ruhl, K. E.; Rovis, T. Photoinduced Ligand-to-Metal Charge Transfer Enables Photocatalyst-Independent Light-Gated Activation of Co(II). *ACS Catal.* **2019**, *9*, 200–204.
- (13) Brauchli, S. Y.; Malzner, F. J.; Constable, E. C.; Housecroft, C. E. Copper(i)-based dye-sensitized solar cells with sterically demanding anchoring ligands: bigger is not always better. *RSC Adv.* **2015**, *5*, 48516–48525.
- (14) Otto, S.; Dorn, M.; Förster, C.; Bauer, M.; Seitz, M.; Heinze, K. Understanding and exploiting long-lived near-infrared emission of a molecular ruby. *Coord. Chem. Rev.* **2018**, *359*, 102–111.
- (15) Chábera, P.; Liu, Y.; Prakash, O.; Thyrahaug, E.; Nahhas, A. E.; Honarfar, A.; Essén, S.; Fredin, L. A.; Harlang, T. C. B.; Kjaer, K. S.; Handrup, K.; Ericson, F.; Tatsuno, H.; Morgan, K.; Schnadt, J.; Häggström, L.; Ericsson, T.; Sobkowiak, A.; Lidin, S.; Huang, P.; Styring, S.; Uhlig, J.; Bendix, J.; Lomoth, R.; Sundström, V.; Persson, P.; Wärnmark, K. A low-spin Fe(III) complex with 100-ps ligand-to-metal charge transfer photoluminescence. *Nature* **2017**, *543*, 695.
- (16) Shields, B. J.; Kudisch, B.; Scholes, G. D.; Doyle, A. G. Long-Lived Charge-Transfer States of Nickel(II) Aryl Halide Complexes Facilitate Bimolecular Photoinduced Electron Transfer. *J. Am. Chem. Soc.* **2018**, *140*, 3035–3039.
- (17) Liu, Y.; Yiu, S.-C.; Ho, C.-L.; Wong, W.-Y. Recent advances in copper complexes for electrical/light energy conversion. *Coord. Chem. Rev.* **2018**, *375*, 514–557.

- (18) Wenger, O. S. Photoactive Complexes with Earth-Abundant Metals. *J. Am. Chem. Soc.* **2018**, *140*, 13522–13533.
- (19) Larsen, C. B.; Wenger, O. S. Photoredox Catalysis with Metal Complexes Made from Earth-Abundant Elements. *Chem. - Eur. J.* **2018**, *24*, 2039–2058.
- (20) Zhang, Y.; Petersen, J. L.; Milsmann, C. A Luminescent Zirconium(IV) Complex as a Molecular Photosensitizer for Visible Light Photoredox Catalysis. *J. Am. Chem. Soc.* **2016**, *138*, 13115–13118.
- (21) Zhang, Y.; Lee, T. S.; Favale, J. M.; Leary, D. C.; Petersen, J. L.; Scholes, G. D.; Castellano, F. N.; Milsmann, C. Delayed fluorescence from a zirconium(IV) photosensitizer with ligand-to-metal charge-transfer excited states. *Nat. Chem.* **2020**, *12*, 345–352.
- (22) Romain, C.; Choua, S.; Collin, J.-P.; Heinrich, M.; Bailly, C.; Karmazin-Brelot, L.; Bellemin-Laponnaz, S.; Dagorne, S. Redox and Luminescent Properties of Robust and Air-Stable N-Heterocyclic Carbene Group 4 Metal Complexes. *Inorg. Chem.* **2014**, *53*, 7371–7376.
- (23) Loukova, G. V.; Huhn, W.; Vasiliev, V.; Smirnov, V. A. Ligand-to-Metal Charge Transfer Excited States with Unprecedented Luminescence Yield in Fluid Solution. *J. Phys. Chem. A* **2007**, *111*, 4117–4121.
- (24) Loukova, G. V.; Milov, A. A.; Vasiliev, V. P.; Minkin, V. I. Dipole moments and solvatochromism of metal complexes: principle photophysical and theoretical approach. *Phys. Chem. Chem. Phys.* **2016**, *18*, 17822–17826.
- (25) Pfennig, B. W.; Thompson, M. E.; Bocarsly, A. B. A New Class of Room Temperature Luminescent Organometallic Complexes: Luminescence and Photophysical Properties of Permethyiscandocene Chloride in Fluid Solution. *J. Am. Chem. Soc.* **1989**, *111*, 8947–8958.
- (26) Turlington, M. D.; Pienkos, J. A.; Carlton, E. S.; Wroblewski, K. N.; Myers, A. R.; Trindle, C. O.; Altun, Z.; Rack, J. J.; Wagenknecht, P. S. Complexes with Tunable Intramolecular Ferrocene to Ti(IV) Electronic Transitions: Models for Solid State Fe(II) to Ti(IV) Charge Transfer. *Inorg. Chem.* **2016**, *55*, 2200–2211.
- (27) Pienkos, J. A.; Agakidou, A. D.; Trindle, C. O.; Herwald, D. W.; Altun, Z.; Wagenknecht, P. S. Titanocene as a New Acceptor (A) for Arylamine Donors (D) in D–A Chromophores. *Organometallics* **2016**, *35*, 2575–2578.
- (28) Pienkos, J. A.; Webster, A. B.; Piechota, E. J.; Agakidou, A. D.; McMillen, C. D.; Pritchett, D. Y.; Meyer, G. J.; Wagenknecht, P. S. Oxidatively stable ferrocenyl-bridge-titanocene D–A complexes: an electrochemical and spectroscopic investigation of the mixed valent state. *Dalton Trans.* **2018**, *47*, 10953–10964.
- (29) Livshits, M. Y.; Turlington, M. D.; Trindle, C. O.; Wang, L.; Altun, Z.; Wagenknecht, P. S.; Rack, J. J. Picosecond to Nanosecond Manipulation of Excited State Lifetimes in Complexes with an Fe^{II} to Ti^{IV} Metal-to-Metal Charge Transfer: The Role of Ferrocene-Centered Excited States. *Inorg. Chem.* **2019**, *58*, 15320–15329.
- (30) Nguyen, K. T.; Lane, E. E.; McMillen, C. D.; Pienkos, J. A.; Wagenknecht, P. S. Is indenyl a stronger or weaker electron donor ligand than cyclopentadienyl? Opposing effects of indenyl electron density and ring slipping on electrochemical potentials. *Organometallics* **2020**, *39*, 670–678.
- (31) Frisch, M. J.; Trucks, G. W.; Schlegel, H. B.; Scuseria, G. E.; Robb, M. A.; Cheeseman, J. R.; Scalmani, G.; Barone, V.; Petersson, G. A.; Nakatsuji, H.; Li, X.; Caricato, M.; Marenich, A. V.; Bloino, J.; Janesko, B. G.; Gomperts, R.; Mennucci, B.; Hratchian, H. P.; Ortiz, J. V.; Izmaylov, A. F.; Sonnenberg, J. L.; Williams-Young, D.; Ding, F.; Lipparini, F.; Egidi, F.; Goings, J.; Peng, B.; Petrone, A.; Henderson, T.; Ranasinghe, D.; Zakrzewski, V. G.; Gao, J.; Rega, N.; Zheng, G.; Liang, W.; Hada, M.; Ehara, M.; Toyota, K.; Fukuda, R.; Hasegawa, J.; Ishida, M.; Nakajima, T.; Honda, Y.; Kitao, O.; Nakai, H.; Vreven, T.; Throssell, K.; Montgomery, J. A., Jr.; Peralta, J. E.; Ogliaro, F.; Bearpark, M. J.; Heyd, J. J.; Brothers, E. N.; Kudin, K. N.; Staroverov, V. N.; Keith, T. A.; Kobayashi, R.; Normand, J.; Raghavachari, K.; Rendell, A. P.; Burant, J. C.; Iyengar, S. S.; Tomasi, J.; Cossi, M.; Millam, J. M.; Klene, M.; Adamo, C.; Cammi, R.; Ochterski, J. W.; Martin, R. L.; Morokuma, K.; Farkas, O.; Foresman, J. B.; Fox, D. J. *Gaussian 16*, revision C.01; Gaussian Inc.: Wallingford, CT, 2016.
- (32) Dennington, R.; Keith, T. A.; Millam, J. M. *GaussView*, version 6; Semichem Inc.: Shawnee Mission, KS, 2016.
- (33) (a) Becke, A. D. Density-functional exchange-energy approximation with correct asymptotic behavior. *Phys. Rev. A: At., Mol., Opt. Phys.* **1988**, *38*, 3098–3100. (b) Lee, C.; Yang, W.; Parr, R. G. Development of the Colle-Salvetti correlation-energy formula into a functional of the electron density. *Phys. Rev. B: Condens. Matter Mater. Phys.* **1988**, *37*, 785–789.
- (34) (a) Becke, A. D. Density-functional thermochemistry. III. The role of exact exchange. *J. Chem. Phys.* **1993**, *98*, 5648–5652. (b) Perdew, J. P.; Chevary, J. A.; Vosko, S. H.; Jackson, K. A.; Pederson, M. R.; Singh, D. J.; Fiolhais, C. Atoms, molecules, solids, and surfaces: Applications of the generalized gradient approximation for exchange and correlation. *Phys. Rev. B: Condens. Matter Mater. Phys.* **1992**, *46*, 6671–6687. (c) Perdew, J. P.; Burke, K.; Wang, Y. Generalized gradient approximation for the exchange-correlation hole of a many-electron system. *Phys. Rev. B: Condens. Matter Mater. Phys.* **1996**, *54*, 16533–16539.
- (35) Grimme, S.; Ehrlich, S.; Goerigk, L. Effect of the damping function in dispersion corrected density functional theory. *J. Comput. Chem.* **2011**, *32*, 1456–65.
- (36) Chai, J.-D.; Head-Gordon, M. Long-range corrected hybrid density functionals with damped atom-atom dispersion corrections. *Phys. Chem. Chem. Phys.* **2008**, *10*, 6615–6620.
- (37) Yanai, T.; Tew, D.; Handy, N. A new hybrid exchange-correlation functional using the Coulomb-attenuating method (CAM-B3LYP). *Chem. Phys. Lett.* **2004**, *393*, 51–57.
- (38) Zhao, Y.; Schultz, N. E.; Truhlar, D. G. Exchange-correlation functional with broad accuracy for metallic and nonmetallic compounds, kinetics, and noncovalent interactions. *J. Chem. Phys.* **2005**, *123*, 161103.
- (39) Zhao, Y.; Truhlar, D. G. The M06 suite of density functionals for main group thermochemistry, thermochemical kinetics, non-covalent interactions, excited states, and transition elements: two new functionals and systematic testing of four M06-class functionals and 12 other functionals. *Theor. Chem. Acc.* **2008**, *120*, 215–241.
- (40) Peverati, R.; Truhlar, D. G. Improving the Accuracy of Hybrid Meta-GGA Density Functionals by Range Separation. *J. Phys. Chem. Lett.* **2011**, *2*, 2810–2817.
- (41) Peverati, R.; Zhao, Y.; Truhlar, D. G. Generalized Gradient Approximation That Recovers the Second-Order Density-Gradient Expansion with Optimized Across-the-Board Performance. *J. Phys. Chem. Lett.* **2011**, *2*, 1991–1997.
- (42) Peverati, R.; Truhlar, D. G. Screened-exchange density functionals with broad accuracy for chemistry and solid-state physics. *Phys. Chem. Chem. Phys.* **2012**, *14*, 16187–16191.
- (43) Peverati, R.; Truhlar, D. G. Screened-Exchange Density Functionals with Broad Accuracy for Chemistry and Solid-State Physics. *Phys. Chem. Chem. Phys.* **2012**, *14*, 16187–16191.
- (44) Yu, H. S.; He, X.; Li, S. L.; Truhlar, D. G. MN15: A Kohn-Sham global-hybrid exchange-correlation density functional with broad accuracy for multi-reference and single-reference systems and noncovalent interactions. *Chem. Sci.* **2016**, *7*, 5032–5051.
- (45) Rassolov, V. A.; Ratner, M. A.; Pople, J. A.; Redfern, P. C.; Curtiss, L. A. 6-31G* Basis Set for Third-Row Atoms. *J. Comput. Chem.* **2001**, *22*, 976–984.
- (46) (a) McLean, A. D.; Chandler, G. S. Contracted Gaussian-basis sets for molecular calculations. 1. 2nd row atoms, Z = 11–18. *J. Chem. Phys.* **1980**, *72*, 5639–5648. (b) Wachters, A. J. H. Gaussian basis set for molecular wavefunctions containing third-row atoms. *J. Chem. Phys.* **1970**, *52*, 1033–1036. (c) Hay, P. J. Gaussian basis sets for molecular calculations-representation of 3D orbitals in transition-metal atoms. *J. Chem. Phys.* **1977**, *66*, 4377–4384. (d) Clark, T.; Chandrasekhar, J.; Spitznagel, G. W.; Schleyer, P. V. R. Efficient diffuse function-augmented basis-sets for anion calculations. 3. The 3-21+G basis set for 1st-row elements, Li-F. *J. Comput. Chem.* **1983**, *4*, 294–301. (e) Frisch, M. J.; Pople, J. A.; Binkley, J. S. Self-Consistent

Molecular Orbital Methods. 25. Supplementary Functions for Gaussian Basis Sets. *J. Chem. Phys.* **1984**, *80*, 3265–3269.

(47) Dunning, T. H.; Hay, P. J. In *Modern Theoretical Chemistry*; Schaefer, H. F., Ed.; Plenum: New York, 1977; Vol. 3, pp 1–28.

(48) Weigend, F.; Ahlrichs, R. Balanced basis sets of split valence, triple zeta valence and quadruple zeta valence quality for H to Rn: Design and assessment of accuracy. *Phys. Chem. Chem. Phys.* **2005**, *7*, 3297–3305.

(49) APEX 3, version 2017.3; Bruker-AXS Inc.: Madison, WI, 2017.

(50) Sheldrick, G. M. Crystal structure refinement with SHELXL. *Acta Crystallogr., Sect. C: Struct. Chem.* **2015**, *71*, 3–8.

(51) Vieira, N. C.; Pienkos, J. A.; McMillen, C. D.; Myers, A. R.; Clay, A. P.; Wagenknecht, P. S. A *trans*-bidentate *bis*-pyridinyl ligand with a transition metal hinge. *Dalton Trans.* **2017**, *46*, 15195–15199.

(52) Choukroun, R.; Donnadieu, B.; Zhao, J.-S.; Cassoux, P.; Lepetit, C.; Silvi, B. Synthesis and Characterization of [Cp₂(m-h²:h⁴-butadiyne)ZrCp'₂] Heterodimetallic Complexes (Cp' = C₅H₄t-Bu, C₅H₄Me). Formation Mechanism and Theoretical (ELF) Evidence for the Existence of Planar Tetracoordinate Carbon (ptC). *Organometallics* **2000**, *19*, 1901–1911.

(53) Back, S.; Stein, T.; Frosch, W.; Wu, I.-Y.; Kralik, J.; Büchner, M.; Huttner, G.; Rheinwald, G.; Lang, H. Heterometallic early-late p-tweezer complexes: their synthesis, electrochemical behaviour and the solid-state structures of [I^{δ-}-C₅H₄SiMe₃]₂Ti(CCPH)₂ and [(^{δ-}-C₅H₄SiMe₃)₂Ti(CCPH)₂]Pd(PPh₃). *Inorg. Chim. Acta* **2001**, *325*, 94–102.

(54) Carlton, E. S.; Sutton, J. J.; Gale, A. G.; Shields, G. C.; Gordon, K. C.; Wagenknecht, P. S. Insights into the charge-transfer character of electronic transitions in ^RCp₂Ti(C₂Fc)₂ complexes using solvatochromism, resonance Raman spectroscopy, and TDDFT. *Dalton Trans.* **2021**, *50*, 2233–2242.

(55) Catalán, J.; Del Valle, J. C. A Spectroscopic Rule from the Solvatochromism of Aromatic Solutes in Nonpolar Solvents. *J. Phys. Chem. B* **2014**, *118*, 5168–5176.

(56) Kenney, J. W.; Boone, D. R.; Striplin, D. R.; Chen, Y. H.; Hamar, K. B. Electronic luminescence spectra of charge transfer states of titanium(IV) metallocenes. *Organometallics* **1993**, *12* (9), 3671–3676.

(57) Patrick, E. L.; Ray, C. J.; Meyer, G. D.; Ortiz, T. P.; Marshall, J. A.; Brozik, J. A.; Summers, M. A.; Kenney, J. W. Non-Localized Ligand-to-Metal Charge Transfer Excited States in (Cp)₂Ti(IV)-(NCS)₂. *J. Am. Chem. Soc.* **2003**, *125* (18), 5461–5470.

(58) (a) Dorn, M.; Kalmbach, J.; Boden, P.; Kruse, A.; Dab, C.; Reber, C.; Niedner-Schatteburg, G.; Lochbrunner, S.; Gerhards, M.; Seitz, M.; Heinze, K. Ultrafast and long-time excited state kinetics of an NIR-emissive vanadium(III) complex I: synthesis, spectroscopy and static quantum chemistry. *Chem. Sci.* **2021**, *12*, 10780. (b) Dorn, M.; Kalmbach, J.; Boden, P.; Pöpcke, A.; Gómez, S.; Förster, C.; Kuczelinis, F.; Carrella, L. M.; Büldt, L. A.; Bings, N. H.; Rentschler, E.; Lochbrunner, S.; González, L.; Gerhards, M.; Seitz, M.; Heinze, K. A Vanadium(III) Complex with Blue and NIR-II Spin-Flip Luminescence in Solution. *J. Am. Chem. Soc.* **2020**, *142*, 7947–7955.

(59) (a) Brintzinger, H. H.; Bercaw, J. E. Nature of so-called titanocene, (C₁₀H₁₀Ti)₂. *J. Am. Chem. Soc.* **1970**, *92*, 6182–6185. (b) Chirik, P. J. Group 4 Transition Metal Sandwich Complexes: Still Fresh after Almost 60 Years. *Organometallics* **2010**, *29*, 1500–1517.

(60) (a) Pez, G. P. Novel conversion of ethylene into ethane and buta-1,3-diene catalysed by titanium metallocenes. *J. Chem. Soc., Chem. Commun.* **1977**, 560–561. (b) Ni, J.; Zhou, Q.; Canseco, D. K.; Calhoun, T. R.; Graham, A. R.; Carreras, K. L.; Schultz, C. N. Transformation of carbon dioxide to methoxide by the complex [(C₅H₅Ti)₂((-H)₂((-C₁₀H₈)). *Inorg. Chim. Acta* **2000**, *309*, 23–27.

(61) Pulst, S.; Arndt, P.; Heller, B.; Baumann, W.; Kempe, R.; Rosenthal, U. Nickel(0) Complexes of Five-Membered Titana- and Zirconacyclocumulenes as Intermediates in the Cleavage of C-C Bonds of Disubstituted Butadiynes. *Angew. Chem., Int. Ed. Engl.* **1996**, *35*, 1112–1115.

(62) Jemmis, E. D.; Phukan, A. K.; Giju, K. T. Dependence of the Structure and Stability of Cyclocumulenes and Cyclopropenes on the

Replacement of the CH₂ Group by Titanocene and Zirconocene: A Density Functional Theory Study. *Organometallics* **2002**, *21*, 2254–2261.

(63) Tomasi, J.; Mennucci, B.; Cammi, R. Quantum Mechanical Continuum Solvation Models. *Chem. Rev.* **2005**, *105*, 2999–3093.

(64) (a) Haehnel, M.; Ruhmann, M.; Theilmann, O.; Roy, S.; Beweries, T.; Arndt, P.; Spannenberg, A.; Villingner, A.; Jemmis, E. D.; Schulz, A.; Rosenthal, U. Reactions of Titanocene Bis(trimethylsilyl)acetylene Complexes with Carbodiimides: An Experimental and Theoretical Study of Complexation versus C-N Bond Activation. *J. Am. Chem. Soc.* **2012**, *134*, 15979–15991. (b) Minasian, S. G.; Keith, J. M.; Batista, E. R.; Boland, K. S.; Kozimor, S. A.; Martin, R. L.; Shuh, D. K.; Tyliczszak, T.; Vernon, L. J. Carbon K-Edge X-ray Absorption Spectroscopy and Time-Dependent Density Functional Theory Examination of Metal-Carbon Bonding in Metallocene Dichlorides. *J. Am. Chem. Soc.* **2013**, *135*, 14731–14740.

(65) Pinkas, J.; Gyepes, R.; Cisařová, I.; Kubiřta, J.; Horáček, M.; Mach, K. Decamethyltitanocene hydride intermediates in the hydrogenation of the corresponding titanocene-(η^2 -ethene) or (η^2 -alkyne) complexes and the effects of bulkier auxiliary ligands. *Dalton Trans.* **2017**, *46*, 8229–8244.

(66) Beaumier, E. P.; Gordon, C. P.; Harkins, R. P.; McGreal, M. E.; Wen, X.; Copéret, C.; Goodpaster, J. D.; Tonks, I. A. Cp₂Ti-(κ^2 -tBuNCN^tBu): A Complex with an Unusual κ^2 Coordination Mode of a Heterocumulene Featuring a Free Carbene. *J. Am. Chem. Soc.* **2020**, *142*, 8006–8018.

(67) Grimme, S.; Antony, J.; Ehrlich, S.; Krieg, H. A consistent and accurate *ab initio* parametrization of density functional dispersion correction (DFT-D) for the 94 elements H-Pu. *J. Chem. Phys.* **2010**, *132*, 154104.

(68) (a) Verma, P.; Truhlar, D. G. Status and Challenges of Density Functional Theory. *Trends Chem.* **2020**, *2*, 302–318. (b) Verma, P.; Wang, Y.; Ghosh, S.; He, X.; Truhlar, D. G. Revised M11 Exchange-Correlation Functional for Electronic Excitation Energies and Ground-State Properties. *J. Phys. Chem. A* **2019**, *123*, 2966–2990.

(69) Niehaus, T. A.; Hofbeck, T.; Yersin, H. Charge-transfer excited states in phosphorescent organo-transition metal compounds: a difficult case for time dependent density functional theory? *RSC Adv.* **2015**, *5*, 63318–63329.

(70) Morello, G. R. Accurate Prediction of Emission Energies with TD-DFT Methods for Platinum and Iridium OLED Materials. *J. Mol. Model.* **2017**, *23*, 174.

(71) Chen, P.; Meyer, T. J. Medium Effects on Charge Transfer in Metal Complexes. *Chem. Rev.* **1998**, *98*, 1439–1477.

(72) Sears, J. S.; Koerzdoerfer, T.; Zhang, C.-R.; Brédas, J.-L. Orbital instabilities and triplet states from time-dependent density functional theory and long-range corrected functionals. *J. Chem. Phys.* **2011**, *135*, 151103.

(73) Davies, D. L.; Lelj, F.; Lowe, M. P.; Ryder, K. S.; Singh, K.; Singh, S. Pyridine imines as ligands in luminescent iridium complexes. *Dalton Trans.* **2014**, *43*, 4026–4039.

(74) Kvapilová, H.; Sattler, W.; Sattler, A.; Sazanovich, I. V.; Clark, I. P.; Towrie, M.; Gray, H. B.; Zálíš, S.; Vlček, A. Electronic Excited States of Tungsten(0) Arylisocyanides. *Inorg. Chem.* **2015**, *54*, 8518–8528.

(75) Collings, J. C.; Parsons, A. C.; Porrès, L.; Beeby, A.; Batsanov, A. S.; Howard, J. A. K.; Lydon, D. P.; Low, P. J.; Fairlamb, I. J. S.; Marder, T. B. Optical properties of donor-acceptor phenylene-ethylene systems containing the 6-methylpyran-2-one group as an acceptor. *Chem. Commun.* **2005**, 2666–2668.

(76) Kasha, M. Characterization of Electronic Transitions in Complex Molecules. *Discuss. Faraday Soc.* **1950**, *9*, 14–19.